Available online at www.sciencedirect.com
ScienceDirect
Journal of Sound and Vibration 319 (2009) 646–667
JOURNAL OF SOUND AND VIBRATION
www.elsevier.com/locate/jsvi

Asymptotic analysis for the coupled wavenumbers in an infinite fluid-filled flexible cylindrical shell: The beam mode

Abhijit Sarkar, Venkata R. Sonti*

Facility for Research in Technical Acoustics, Department of Mechanical Engineering, Indian Institute of Science, Bangalore 560 012, India

Received 12 September 2007; received in revised form 6 June 2008; accepted 8 June 2008
Handling Editor: L.G. Tham
Available online 29 July 2008

Abstract

Using asymptotics, the coupled wavenumbers in an infinite fluid-filled flexible cylindrical shell vibrating in the beam mode (*viz.* circumferential wave order $n = 1$) are studied. Initially, the uncoupled wavenumbers of the acoustic fluid and the cylindrical shell structure are discussed. Simple closed form expressions for the structural wavenumbers (longitudinal, torsional and bending) are derived using asymptotic methods for low- and high-frequencies. It is found that at low frequencies the cylinder in the beam mode behaves like a Timoshenko beam. Next, the coupled dispersion equation of the system is rewritten in the form of the uncoupled dispersion equation of the structure and the acoustic fluid, with an added fluid-loading term involving a parameter μ due to the coupling. An asymptotic expansion involving μ is substituted in this equation. Analytical expressions are derived for the coupled wavenumbers (as modifications to the uncoupled wavenumbers) separately for low- and high-frequency ranges and further, within each frequency range, for large and small values of μ. Only the flexural wavenumber, the first rigid duct acoustic cut-on wavenumber and the first pressure-release acoustic cut-on wavenumber are considered. The general trend found is that for small μ, the coupled wavenumbers are close to the *in vacuo* structural wavenumber and the wavenumbers of the rigid-acoustic duct. With increasing μ, the perturbations increase, until the coupled wavenumbers are better identified as perturbations to the pressure-release wavenumbers. The systematic derivation for the separate cases of small and large μ gives more insight into the physics and helps to continuously track the wavenumber solutions as the fluid-loading parameter is varied from small to large values. Also, it is found that at any frequency where two wavenumbers intersect in the uncoupled analysis, there is no more an intersection in the coupled case, but a gap is created at that frequency. This method of asymptotics is simple to implement using a symbolic computation package (like Maple).

1. Introduction

Wave propagation in fluid-filled cylindrical shells is a classical topic of interest to the structural acoustics community. This is evidenced by the large volume of literature on the subject. In contrast to the planar fluid–structure interaction problems, the fluid–shell system poses an additional challenge by having the motion in the three coordinate directions coupled due to the shell curvature. In this context, the efforts of some

*Corresponding author.
E-mail address: sonti@mecheng.iisc.ernet.in (V.R. Sonti).

0022-460X/$ - see front matter © 2008 Elsevier Ltd. All rights reserved.
doi:10.1016/j.jsv.2008.06.008

researchers have been in finding the fluid-shell coupled wavenumbers. They have numerically solved the coupled dispersion equation by varying individual parameters [1–4] and also discussed the physics related to the coupled wavenumbers. However, this numerical root-finding approach is laborious, and the solutions are not amenable to easy understanding. For example, to understand the influence of the fluid on the structure or *vice versa*, an analytical expression for the coupled wavenumbers would be very useful. It would then be easy to identify the coupled wavenumbers as a modification to the uncoupled wavenumbers. To this end, the method of asymptotics appears to be a seemingly indispensable approach as it leads to analytical expressions for the coupled wavenumbers, which conveniently are perturbations to the uncoupled wavenumbers.

The essence of asymptotic analysis is to arrive at a solution for a complicated system which in *some way* is near to a solvable simpler system with known analytical solutions. Using asymptotics, analytical expressions can be found for the complicated system also and these expressions are slightly modified (or perturbed) versions of those of the simpler system. This method is widely prevalent in solving for weakly nonlinear systems [5]. The method has also been widely used in the field of nonlinear acoustics [6].

Defining the fluid-loading effect in the form of a perturbation parameter, asymptotic analysis has been used to analyze structures in contact with infinite acoustic domains for plane [7–9] and cylindrical [10,11] geometries. In contrast, for systems with finite acoustic domains, such as a flexible acoustic duct, studies have been mainly of experimental [12–14] or of numerical [1,2,15,16] nature. Applications of the asymptotic method to flexible acoustic ducts have not come to our notice. Studies using asymptotic methods to find the coupled wavenumbers of structural acoustic systems in two different geometries have been recently carried out by us [17,18].

In this study, we consider an infinite fluid-filled flexible circular cylindrical shell (see Fig. 1). Our interest is to find the coupled structural acoustic wavenumbers for this system as perturbations to the uncoupled structural and the acoustic wavenumbers. Numerical solutions to this problem have already been presented [1]. Here, we wish to bring more insight into the character of the wavenumber solutions using asymptotics.

As a representative case, we choose to study the beam mode (*viz.* circumferential wave order $n = 1$) in detail in the present article. The higher order circumferential modes ($n > 1$) closely resemble this mode (in a qualitative sense) [19]. Further, $n = 1$ mode is the lowest order mode in which the vibrations in all three directions (*viz.* radial, longitudinal and torsional) are coupled. In contrast, for the axisymmetric mode the

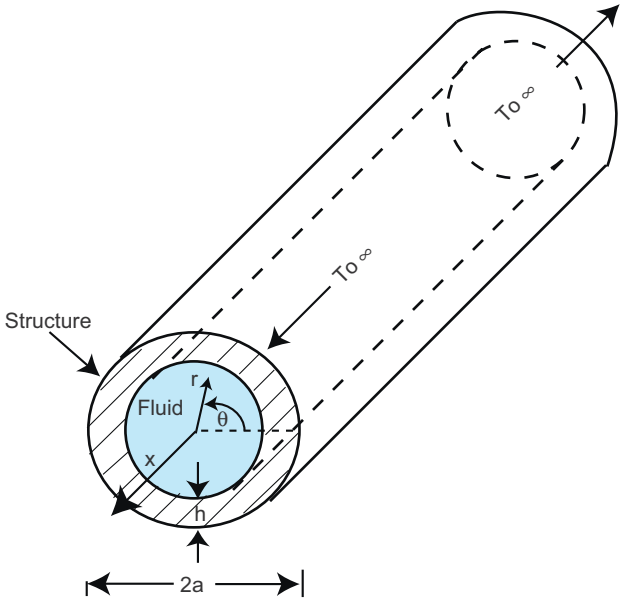

Fig. 1. Schematic of the model showing the fluid-filled flexible cylindrical shell of infinite length. The cylindrical coordinate system (r, θ, x) used for the study is also shown.

torsional displacement is uncoupled from the other two. For the axisymmetric mode, we have found analytical expressions for the coupled wavenumbers using asymptotic methods [18].

For the acoustic fluid in a cylindrical duct, simple closed form expressions for the wavenumbers in the $n = 1$ mode are well-known. However, the dispersion relation for the cylindrical shell is an unwieldy polynomial equation. Hence, in the first part of the article, simple expressions for the *in vacuo* shell wavenumbers will be derived for low and high frequencies using asymptotics. In the process of derivation, we will show that at low frequencies the uncoupled shell (equivalently the *in vacuo* shell) behaves as a Timoshenko beam, whereas at high frequencies the shell resembles a plate of identical thickness [19].

Next, it will be shown that the dispersion relation of the coupled system is related to the uncoupled structural and acoustic system through a fluid-loading parameter. Using this as the perturbation parameter, we will find the coupled wavenumber expressions for small and large fluid-loading. The inherent nature of the asymptotic method provides analytical expressions for the coupled wavenumbers in terms of the uncoupled wavenumber expressions and a correction factor involving the fluid-loading parameter.

2. Uncoupled analysis

In this section, we shall derive expressions for the wavenumbers of the acoustic medium in a cylindrical duct and the wavenumbers of an infinite cylindrical shell vibrating in vacuum. These shall be referred to as the uncoupled acoustic and structural wavenumbers, respectively. Note, the uncoupled structural wavenumber is simply the *in vacuo* wavenumber. On the other hand, the uncoupled acoustic wavenumber is the wavenumber of the acoustic wave in the infinite cylindrical duct. This wavenumber depends on the acoustic boundary condition on the cylinder walls and can have two forms: the first when the cylinder wall is rigid (acoustic velocity is zero) and the second when the cylinder wall has a pressure-release condition (acoustic pressure is zero). The uncoupled acoustic wavenumber is presented in these two forms because as will be seen later, the coupled wavenumbers will turn out to be perturbations to these two forms under various situations. Throughout the article a harmonic time dependence of the form $e^{-i\omega t}$ is assumed. Further, in this article we shall find only the real positive wavenumbers which correspond to waves traveling in the $+x$ direction.

2.1. The uncoupled acoustic wavenumbers (κ_1^r and κ_1^p)

A wave solution traveling in the $+x$ direction for the acoustic pressure (p) in the $n = 1$ mode is given by [7]

$$p(r,\theta,x,t) = PJ_1(k_s r)\cos(\theta)e^{ik_x x}e^{-i\omega t},$$

where the arbitrary constant P gives the amplitude and J_1 denotes the first-order Bessel function of the first kind. Denoting the sonic velocity of the medium by c_f, the values of k_s and k_x for the first rigid-walled and pressure-release cut-on modes are given in Table 1. The non-dimensional axial wavenumber ($k_x a$) corresponding to these two waves will be denoted by κ_1^r and κ_1^p, respectively. Note, to satisfy the rigid-walled or the pressure-release boundary condition on the cylinder wall we have

$$J_1'(k_s a) = 0, \quad \text{for a rigid-walled cylindrical duct and} \tag{1a}$$

$$J_1(k_s a) = 0, \quad \text{for a pressure release cylindrical duct.} \tag{1b}$$

Table 1
Non-dimensional wavenumbers for the first cut-on mode of a cylindrical duct, with $n = 1$, under different boundary conditions

Mode	$k_s a$	Non-dimensionalised wavenumber ($k_x a$)
First rigid-walled	1.841	$\kappa_1^r = \sqrt{\frac{\omega^2 a^2}{c_f^2} - 1.841^2}$
First pressure-release	3.832	$\kappa_1^p = \sqrt{\frac{\omega^2 a^2}{c_f^2} - 3.832^2}$

The presence of a flexible structure modifies the boundary conditions and hence these wavenumbers κ_1^r and κ_1^p. In Section 3, the modified wavenumbers corresponding to these two waves will be found using asymptotics.

2.2. Uncoupled structural wavenumbers

Using the Donell–Mushtari theory [20], the non-dimensional governing equation for the *in vacuo* free vibration in the beam mode of an infinite cylindrical shell of radius a, thickness h, at a circular frequency ω is given by

$$\overbrace{\begin{bmatrix} -\Omega^2+\kappa^2+\frac{1-\nu}{2} & \frac{1}{2}(1+\nu)\kappa & \nu\kappa \\ \frac{1}{2}(1+\nu)\kappa & -\Omega^2+\frac{1-\nu}{2}\kappa^2+1 & 1 \\ \nu\kappa & 1 & -\Omega^2+1+\beta^2(\kappa^2+1)^2 \end{bmatrix}}^{\mathbf{L}} \begin{Bmatrix} u \\ v \\ w \end{Bmatrix} = \begin{Bmatrix} 0 \\ 0 \\ 0 \end{Bmatrix}, \tag{2}$$

where u, v, w are the vibrational amplitudes in the axial, circumferential and radial directions, respectively. The shell material has a Poisson's ratio ν and an extensional wave speed of c_L. The 3×3 square matrix in the equation above shall be referred to as $\mathbf{L}$. The non-dimensional terms in $\mathbf{L}$ are given by $\Omega=\omega a/c_L$, $\beta^2=h^2/12a^2$ and $\kappa=k_x a$.

It is apparent from the non-diagonal form of $\mathbf{L}$ that the essential complication introduced due to the shell curvature is coupling of the motions in the three perpendicular directions. The radial and circumferential directions are kinematically coupled through the curvature. The axial and radial vibrations are coupled due to the Poisson's effect [21].

The free wavenumbers are obtained by equating the determinant of $\mathbf{L}$ to zero (*viz.*, the dispersion equation) and solving for κ. Using the Donell–Mushtari model, the dispersion relation for the *in vacuo* cylindrical shell is given by

$$\begin{aligned} &(-\tfrac{1}{2}\nu\beta^2+\tfrac{1}{2}\beta^2)\kappa^8+(-\tfrac{3}{2}\Omega^2\beta^2-2\nu\beta^2+\tfrac{1}{2}\nu\Omega^2\beta^2+2\beta^2)\kappa^6\\ &\quad+(\tfrac{1}{2}\nu\Omega^2+\Omega^4\beta^2-3\nu\beta^2-\tfrac{9}{2}\Omega^2\beta^2+\tfrac{1}{2}-\tfrac{1}{2}\nu^2+\tfrac{1}{2}\nu^3+\tfrac{3}{2}\nu\Omega^2\beta^2+3\beta^2-\tfrac{1}{2}\nu-\tfrac{1}{2}\Omega^2)\kappa^4\\ &\quad+(2\Omega^4\beta^2-\tfrac{1}{2}\nu\Omega^4+\tfrac{3}{2}\nu\Omega^2-2\nu\beta^2-\tfrac{9}{2}\Omega^2\beta^2+\nu^2\Omega^2+\tfrac{3}{2}\nu\Omega^2\beta^2-\tfrac{5}{2}\Omega^2+2\beta^2+\tfrac{3}{2}\Omega^4)\kappa^2\\ &\quad+(\Omega^4\beta^2+\tfrac{5}{2}\Omega^4-\Omega^6-\tfrac{1}{2}\nu\Omega^4-\tfrac{1}{2}\nu\beta^2+\tfrac{1}{2}\beta^2-\tfrac{3}{2}\Omega^2\beta^2+\tfrac{1}{2}\nu\Omega^2\beta^2+\nu\Omega^2-\Omega^2)=0. \end{aligned} \tag{3}$$

The equation above is an eighth-order polynomial equation in κ and therefore there are four wavenumber solutions (modulo sign) at every frequency. Fuller [19] numerically solved the equation and presented the free wave characteristics of the four wavenumber branches. Three of these wavenumbers are real corresponding to propagating waves.

In the following, we shall find the asymptotic expressions for the real wavenumbers arising from Eq. (3). These shall be denoted by κ_B, κ_L and κ_T for the bending, longitudinal and torsional wavenumbers, respectively. Separate expressions will be derived for high and low frequencies. To our knowledge, these expressions have not been presented so far in the literature. In Section 3, when the coupled wavenumber expressions are derived, they will turn out to be perturbations to these uncoupled wavenumber expressions.

2.2.1. Structural wavenumbers at high frequencies ($\kappa_B, \kappa_L, \kappa_T$)

For modeling the dynamics at high frequencies, we substitute $\Omega=\Omega'/\varepsilon$, where $0<\varepsilon\ll 1$ and Ω' is an $\mathcal{O}(1)$ quantity. We know that the longitudinal and torsional wavenumbers are directly proportional to the frequency. Thus, the wavenumbers in these cases are appropriately scaled as $\kappa=k/\varepsilon$ (k being an $\mathcal{O}(1)$ quantity). However, the flexural wavenumber being proportional to the square root of Ω, is scaled as $\kappa=k/\sqrt{\varepsilon}$.

Using these substitutions in Eq. (3) and employing a regular perturbation method [5] with ε as the perturbation parameter, we find the wavenumber solutions for the high frequency range (given by Eqs. (4)–(6)).

Details of the derivation for the bending wavenumber are shown in Box 1, while Box 2 contains the derivation for the torsional and the longitudinal wavenumbers.

In Fig. 2, an overlaid plot of the above solutions (Eqs. (4)–(6)), along with the numerical solution of the dispersion Eq. (3) is presented. The parameters chosen are $h/a = 0.05$ and $\nu = 0.25$. Unless, otherwise mentioned these structural parameter values shall be used for all subsequent plots.

Box 1

Derivation of the asymptotic expressions for the *in vacuo* bending wavenumber of a cylindrical shell vibrating in the beam mode ($n = 1$) at high frequencies.

We substitute $\Omega = \Omega'/\epsilon$, $\kappa = k/\sqrt{\epsilon}$ in equation (3). In the resulting expression we put $k = a_0 + a_1\epsilon$ and perform a series expansion about ϵ to get

$$-\Omega'^6 + \Omega'^4\beta^2 a_0^4 + [2\Omega'^4\beta^2 a_0^2 + \tfrac{1}{2}\Omega'^2 a_0^6\nu\beta^2 + 4\Omega'^4\beta^2 a_0^3 a_1 + \tfrac{3}{2}\Omega'^4 a_0^2 - \tfrac{1}{2}\Omega'^4 a_0^2\nu - \tfrac{3}{2}\Omega'^2 a_0^6\beta^2]\epsilon + \mathcal{O}(\epsilon^2) = 0.$$

Balancingterms at $\mathcal{O}(1)$ we get $a_0 = \pm\sqrt{\frac{\Omega'}{\beta}}$. Using this in the $\mathcal{O}(\epsilon)$ term we get $a_1 = -\frac{1}{2}\sqrt{\frac{\beta}{\Omega'}}$. Thus,

$$k = \sqrt{\frac{\Omega'\epsilon}{\beta}} - \tfrac{1}{2}\sqrt{\frac{\beta}{\Omega'\epsilon}}\epsilon$$

Hence, the flexural wavenumber for high frequencies (denoted by κ_B) is given by

$$\kappa_B = \sqrt{\frac{\Omega}{\beta}} - \tfrac{1}{2}\sqrt{\frac{\beta}{\Omega}} \tag{4}$$

Box 2

Derivation of the asymptotic expressions for the *in vacuo* longitudinal and torsional wavenumbers of a cylindrical shell vibrating in the beam mode ($n = 1$) at high frequencies.

We substitute $\Omega = \Omega'/\epsilon$ and $\kappa = k/\epsilon$ in equation (3). In the resulting expression we put $k = a_0 + a_2\epsilon^2$ and perform a series expansion about ϵ to get an equation involving various orders of ϵ. Solving the $\mathcal{O}(1)$ equation we get $a_0 = \pm\Omega', \pm\sqrt{\frac{2}{1-\nu}}\Omega'$. Putting $a_0 = \Omega'$, the solution for the $\mathcal{O}(\epsilon^2)$ equation gives $a_2 = -\frac{1}{2\Omega'}$. Thus, we get the wavenumber corresponding to the longitudinal wave (denoted by κ_L) as

$$k = \Omega' - \frac{1}{2\Omega'}\epsilon^2, \Rightarrow \kappa_L = \Omega - \frac{1}{2\Omega}. \tag{5}$$

Similarly,putting $a_0 = \sqrt{\frac{2}{1-\nu}}\Omega'$, the solution for the $\mathcal{O}(\epsilon^2)$ equation gives

$$a_2 = \frac{1}{32}\frac{(2-2\nu)^{7/2}}{(-1+3\nu-3\nu^2+\nu^3)\Omega'}.$$

Thus, the wavenumber corresponding to the torsional wave is given by

$$\kappa_T = \sqrt{\frac{2}{1-\nu}}\Omega + \frac{1}{32}\frac{(2-2\nu)^{7/2}}{(-1+3\nu-3\nu^2+\nu^3)\Omega}. \tag{6}$$

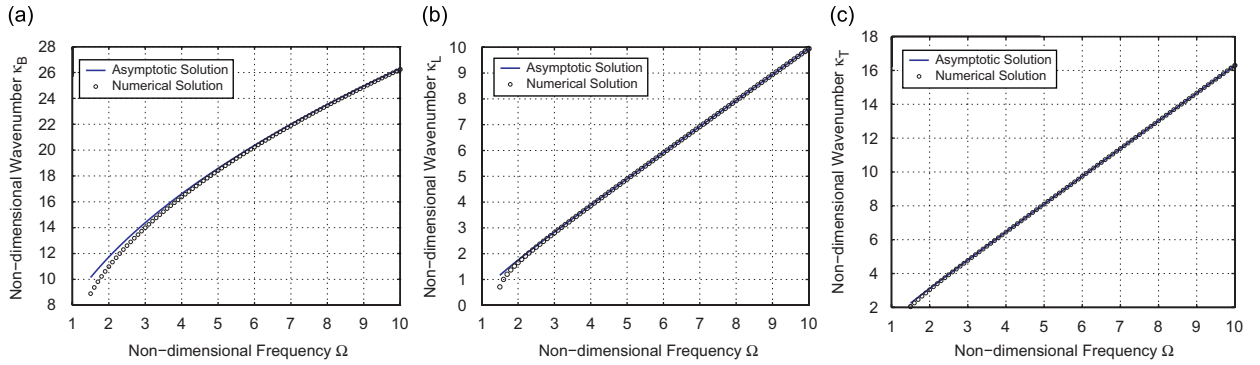

Fig. 2. *In vacuo* wavenumbers for an infinite cylindrical shell with $h/a = 0.05$ and $\nu = 0.25$ (a) bending wavenumber given by equation (4) (b) longitudinal wavenumber given by equation (5) (c) torsional wavenumber given by equation (6).

2.2.2. *Bending wavenumber at low frequencies* ($\underline{\kappa_B}$)

At low frequencies, the *in vacuo* cylindrical shell vibrating in the first circumferential mode ($n = 1$) has only one propagating (real) wavenumber. This wavenumber (denoted by $\underline{\kappa_B}$) is close to the wavenumber of a beam with an annular cross-section of radius a and thickness h [19]. In the following, using the shell equations, we shall find an asymptotic expression for $\underline{\kappa_B}$ for small values of the shell thickness parameter.

From the Euler–Bernoulli beam theory, the bending wavenumber for a beam with annular cross-section of radius a and thickness h is found to be $2^{1/4}\sqrt{\Omega}$ (see Fahy [22] for details). Using Rayleigh theory, which includes the rotary inertia of the beam cross-section but neglects the shear deformation, the dispersion relation for the beam is given by [23,24]

$$\kappa^4 - \Omega^2\kappa^2 - 2\Omega^2 = 0. \tag{7}$$

Also, the dispersion relation for the beam using Timoshenko beam theory is [25]

$$\kappa^4 - \left[1 + \frac{2(1+\nu)}{k}\right]\kappa^2\Omega^2 - 2\Omega^2 + \frac{2(1+\nu)\Omega^4}{k} = 0, \tag{8}$$

where, $k = 2(1+\nu)/(4+3\nu)$ is the shear coefficient for the beam cross-section [26]. The one and two term asymptotic expressions for $\underline{\kappa_B}$ will be shown to be close to the wavenumbers predicted by the Euler–Bernoulli and the Timoshenko theories, respectively.

To capture the low-frequency behavior, we scale Ω as $\varepsilon\Omega'$, where $0 < \varepsilon \ll 1$ is a small quantity and Ω' is an $\mathcal{O}(1)$ quantity. To find the wavenumber near the bending wavenumber, we scale the non-dimensional wavenumber as $\kappa = \sqrt{\varepsilon}k$. Physically, we know that the wavenumber we are looking for exists for small values of the shell thickness parameter (β). We incorporate this into the model by assuming $\beta = \varepsilon b$. Making these substitutions in Eq. (3) and using a regular perturbation method with ε as the perturbation parameter, we get the bending wavenumber for low frequencies as given in Eq. (9). Details of the derivation are shown in Box 3.

The numerical solution of Eq. (3) (Donell–Mushtari model) is compared with the Flugge model solution in Fig. 3 (see Ref. [20] for the Flugge model). Overlaid on the plot are the wavenumbers obtained from the Euler–Bernoulli, the Rayleigh (solution of Eq. (7)) and the Timoshenko (solution of Eq. (8)) beam model. It is observed that the one-term approximation matches with the wavenumber obtained from the Euler–Bernoulli beam model, whereas the two-term approximation is in agreement with the shell theory and the Timoshenko theory for low frequencies ($\Omega < 0.4$).

As observed by Forsberg [27], for beam-type vibrations of circular cylindrical shells, the shell theory *automatically* includes the rotary inertia and the shear deformation effects on the overall cross-section. Hence, the shell theory results match with the results of the Timoshenko model.

In Fig. 4, the bending wavenumber is plotted for the entire frequency range. For low frequencies ($\Omega < 0.5$) we use the asymptotic expression (9), whereas for high frequencies ($\Omega > 3$) we use the asymptotic expression in Eq. (4). In the intermediate range, the roots are found by numerical solution. It may be observed from the plot

Box 3

Derivation of the asymptotic expressions for the *in vacuo* bending wavenumbers of a cylindrical shell vibrating in the beam mode ($n = 1$) at low frequencies.

We substitute $\Omega = \epsilon\Omega'$, $\beta = \epsilon b$ and $\kappa = \sqrt{\epsilon}k$ in Eq. (3). In the resulting expression we put $k = k_0 + \epsilon k_1$ and perform a series expansion about ϵ. Collecting coefficients at each order of ϵ, we find

$$(\nu\Omega'^2 - \tfrac{1}{2}\nu^2 k_0^4 - \tfrac{1}{2}\nu k_0^4 + \tfrac{1}{2}\nu^3 k_0^4 - \Omega'^2 + \tfrac{1}{2}b^2 - \tfrac{1}{2}\nu b^2 + \tfrac{1}{2}k_0^4) + (2k_0^3 k_1 + 2b^2 k_0^2 + \nu^2\Omega'^2 k_0^2 - 2\nu^2 k_0^3 k_1 + \tfrac{3}{2}\nu\Omega'^2 k0^2 - 2\nu b^2 k_0^2 - 2\nu k_0^3 k_1 + 2\nu^3 k_0^3 k_1 - \tfrac{5}{2}\Omega'^2 k_0^2)\epsilon + \mathcal{O}(\epsilon^2) = 0.$$

Equating coefficients at $\mathcal{O}(1)$ we get $k_0 = \sqrt[4]{(2\Omega'^2 - b^2)/(1-\nu^2)}$. Using this value of k_0 and equating coefficients at $\mathcal{O}(\epsilon)$, we get $k_1 = -\frac{1}{4}\frac{1}{\sqrt[4]{(-2\Omega'^2+b^2)/(\nu^2-1)}}\frac{(2\nu\Omega'^2-4b^2+5\Omega'^2)}{\nu^2-1}$.

Having obtained k (from k_0 and k_1), we resubstitute $\Omega' = \Omega/\epsilon$, $b = \beta/\epsilon$ and $k = \kappa/\sqrt{\epsilon}$, to get κ. The following two cases arise depending on whether we take a one or two term approximation for k:

$$\underline{\kappa_B} = \begin{cases} \sqrt[4]{\dfrac{2\Omega^2-\beta^2}{1-\nu^2}} - \dfrac{(2\nu\Omega^2 - 4\beta^2 + 5\Omega^2)}{4(\nu^2-1)}\dfrac{1}{\sqrt[4]{\dfrac{2\Omega^2-\beta^2}{1-\nu^2}}} & \text{two-term approximation,} \\ \sqrt[4]{\dfrac{2\Omega^2-\beta^2}{1-\nu^2}} & \text{one-term approximation.} \end{cases} \quad (9)$$

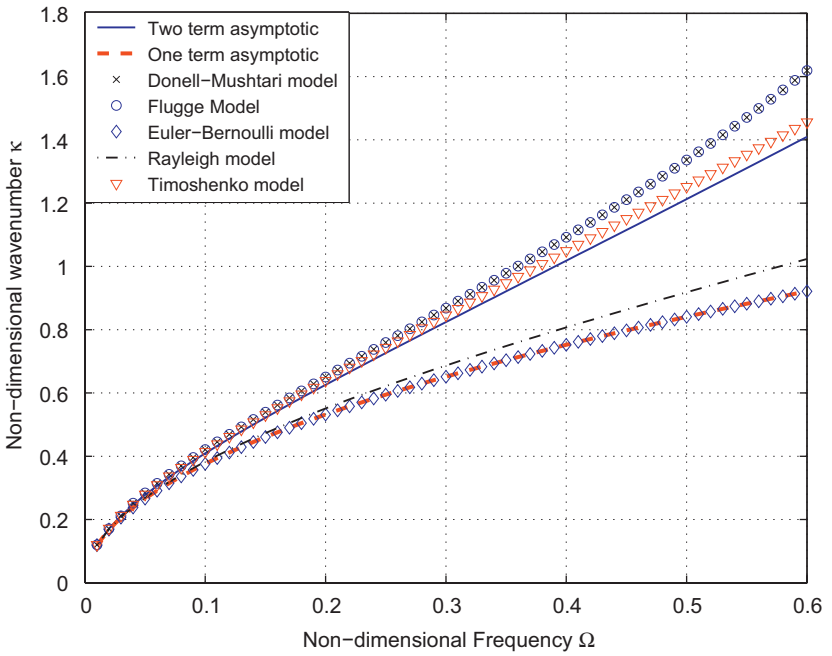

Fig. 3. Low frequency *in vacuo* bending wavenumber for an infinite cylindrical shell with $h/a = 0.05$ and $\nu = 0.25$.

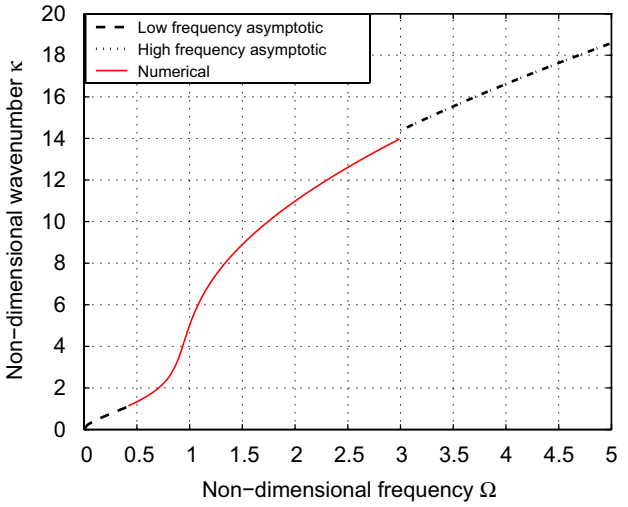

Fig. 4. *In vacuo* bending wavenumber for an infinite cylindrical shell with $h/a = 0.05$ and $\nu = 0.25$.

that around $\Omega \approx 1$, the nature of the transverse wave changes from the bending wave in a beam with an annular cross section of radius a and thickness h ($h \ll a$) to flexural waves in a plate of thickness h [19].

3. The coupled problem

The derivation of the coupled dispersion relation in a fluid-filled cylindrical shell for a general circumferential mode of order n has been presented by Fuller and Fahy [1]. The governing differential equation for an infinite fluid-filled cylindrical shell is given by Eq. (2) with the L_{33} term modified as shown below

$$L_{33} = -\Omega^2 + 1 + \beta^2(\kappa^2+1)^2 - \underbrace{\frac{\Omega^2}{\xi}\overbrace{\left(\frac{\rho_f a}{\rho_s h}\right)}^{\mu}\frac{J_1(\xi)}{J_1'(\xi)}}_{=\mathscr{F}}, \quad \text{where } \xi = \sqrt{\left(\frac{c_L}{c_f}\right)^2\Omega^2 - \kappa^2}. \tag{10}$$

The coupled dispersion equation is thus obtained as

$$|\mathbf{L}| = 0, \tag{11}$$

where L_{33} is given by Eq. (10) and all other components are given by Eq. (2). For brevity, we use the notations $\mathscr{F}$, μ and ξ as indicated in Eq. (10). The ratio of extensional wave speed in the structure to the acoustic wave speed in the fluid will be denoted by c. As seen from Eq. (10), the fluid loading term directly affects the flexural equation. Hence, in the following we shall confine our interest to flexural waves.

Depending on the value of c (*viz.* c_L/c_f), the following situations can arise:

1. The acoustic cut-on intersects the *in vacuo* structural wavenumber branch only at a high frequency. For none of the cut-ons is there an intersection between the wavenumber branches at low frequencies. This happens when for a fixed structure, the sound speed is relatively high. This is demonstrated in Fig. 5a for the first and the second rigid-duct cut-ons.
2. For the other extreme, *viz.* when $c \gg 1$, the acoustic cut-on frequency is lowered. Hence, the coincidence between the lower order acoustic cut-ons and the *in vacuo* structural wavenumber occurs at a low frequency. However, the higher order cut-on branches intersect with the *in vacuo* structural wavenumber branch at high frequencies. Fig. 5b shows the low frequency first and second cut-ons along with a high eighth-order cut-on wavenumber.

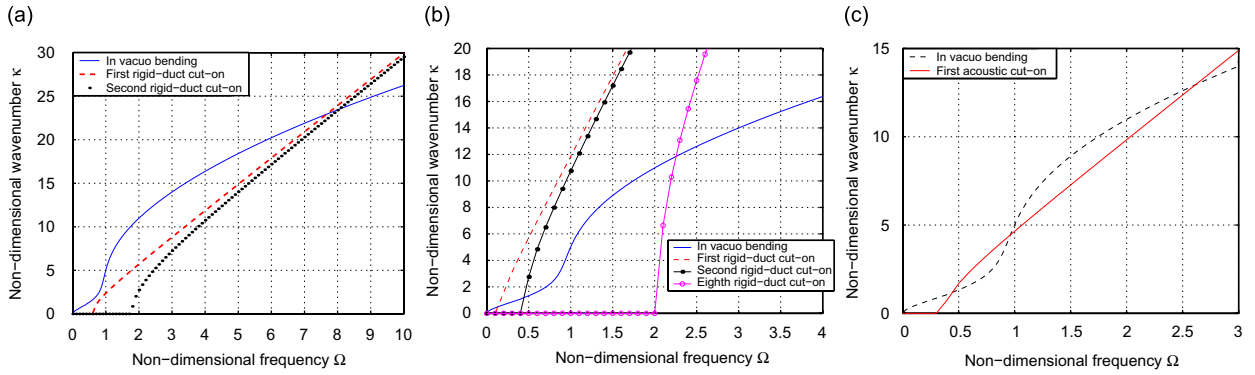

Fig. 5. Various coincidence conditions possible between the flexural wavenumber and the acoustic wavenumbers. Parameters chosen are $h/a = 0.05$ and $\nu = 0.25$: (a) $c_L/c_f = 3$, (b) $c_L/c_f = 12$ and (c) $c_L/c_f = 5$.

Table 2
Notation for the uncoupled wavenumbers and the corresponding coupled wavenumbers

Wavenumber	Uncoupled		Coupled	
	High frequency	Low frequency	High frequency	Low frequency
in vacuo bending	κ_B	$\underline{\kappa_B}$	$\kappa_B(\mu)$	$\underline{\kappa_B(\mu)}$
First rigid acoustic cut-on	κ_1^r		$\kappa_1^r(\mu)$	
First pressure-release acoustic cut-on	κ_1^p		$\kappa_1^p(\mu)$	

3. For intermediate values of c, the acoustic wavenumber of a lower order cut-on mode may intersect the *in vacuo* structural wavenumber branch at three frequencies: the first higher than unity, the second near unity and the third lower than unity. This is demonstrated in Fig. 5c for $c = 5$ for the first rigid-duct cut on mode. Note, in this case also the higher order modes intersect the structural wavenumber at higher frequencies only.

In this article, the coupled wavenumbers of the system in Fig. 1 are sought as perturbations to the uncoupled wavenumbers found in Section 2. The perturbation will be a function of the fluid-loading parameter μ. We follow a naming convention for the coupled waves. For example, the coupled wavenumber branch which is near the *in vacuo* structural wavenumber will be referred to as the "coupled structural wavenumber", and so on. See Table 2 for notation. Further, in this article, only the coupled structural wavenumber and the first acoustic cut-on (rigid-duct and pressure-release) will be presented. The methodology for the higher order cut-ons is essentially the same.

For numerical validation, as in Section 2, the structural parameter values $h/a = 0.05$ and $\nu = 0.25$ are used for all plots to be presented later. So as to get two extreme coincidence conditions discussed above (items 1 and 2), the values $c = 3$ and 12 will be used. Just as was done for the uncoupled structural wavenumbers in Section 2.2, the asymptotics on the coupled wavenumbers will be presented separately for the low- and high-frequency ranges.

As discussed earlier, depending on the value of c, the coincidence between the structural and the acoustic waves occurs at low or at high frequencies (indicated in Fig. 6 left side). Hence, the derivations to follow are partitioned into a high- and a low-frequency section, each one further having a small μ and a large μ section (indicated in Fig. 6 top right side). By using order analysis arguments separately for the high and the low frequencies, the unwieldy coupled dispersion relation will be simplified. Next, for each frequency range, separate asymptotic expansions will be found for small and large values of μ. For both the high- and low-frequency ranges, the following results shall be found through the subsequent derivations (a) with small μ, the coupled wavenumbers are perturbations to the *in vacuo* bending wavenumber and the wavenumbers of the

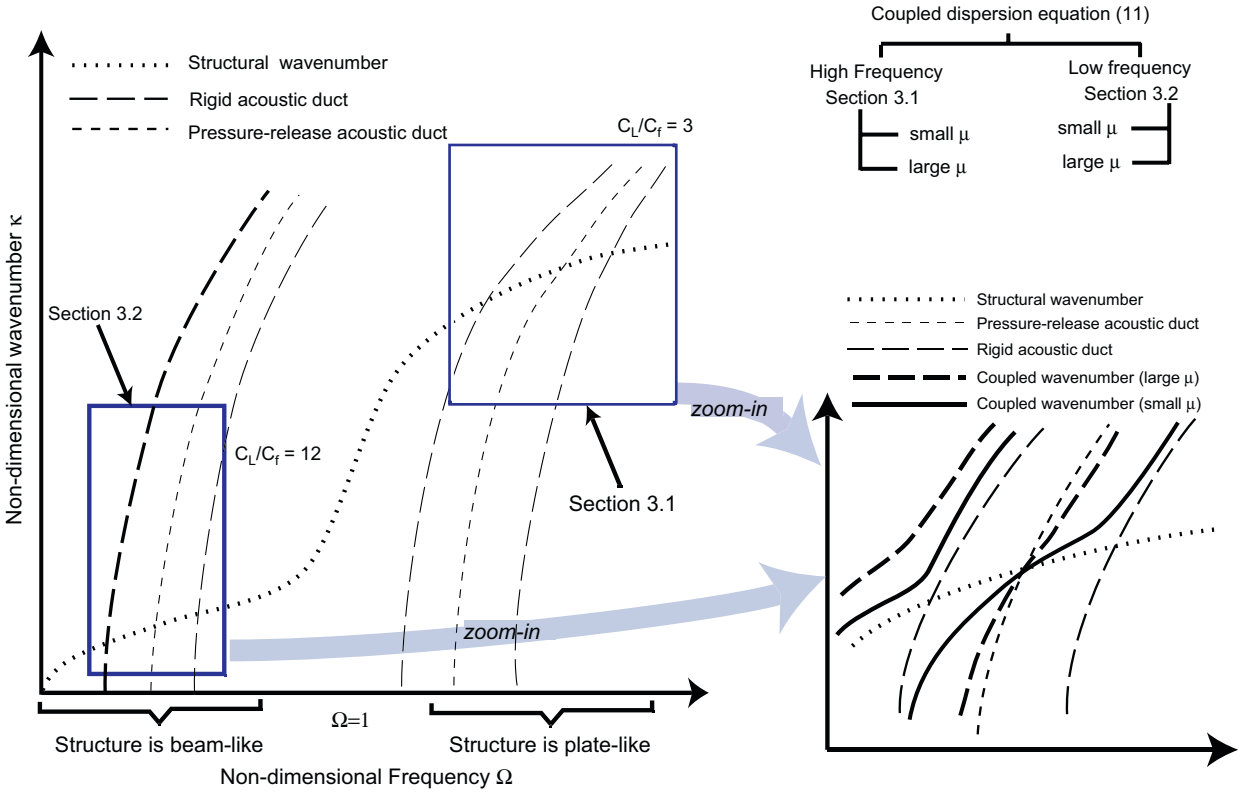

Fig. 6. Structuring of Section 3. The right bottom schematic shows a zoomed-in view of the coupled wavenumbers to be derived for both the high- and the low-frequency regions.

rigid acoustic cut-on (b) with large μ, the coupled wavenumbers are perturbations to the wavenumbers of the pressure-release acoustic cut-ons. This common characteristics of the coupled wavenumbers for both the high- and low-frequency ranges is indicated schematically in a common inset picture (on the bottom right side) in Fig. 6. Accompanying each numerical result in a subsection, a similar relevant schematic diagram will be presented indicating the results found in that subsection.

3.1. High-frequency range

At high frequencies (and hence at high wavenumbers), an order analysis argument is used to simplify the coupled dispersion Eq. (11). This is explained in Box 4.

With the simplifications shown in Box 4, the coupled dispersion equation is given by

$$\overbrace{(-\Omega^2+\kappa^2)}^{L}\underbrace{\left(-\Omega^2+\frac{1-\nu}{2}\kappa^2\right)}_{T}\left[\overbrace{(-\Omega^2+\beta^2\kappa^4)}^{B}\,\xi\,\overbrace{J_1'(\xi)}^{R}-\mu\Omega^2\underbrace{J_1(\xi)}_{P}\right]=0,\ \text{where}\ \mu=\frac{\rho_f a}{\rho_s h}. \tag{13}$$

The physical relevance of each term in the equation above is described as follows:

1. The roots of L represent the wavenumbers of the longitudinal wave in the shell wall in the high-frequency limit. This is the first-order term in Eq. (5).
2. The roots of T represent the wavenumbers of the torsional wave. This is the first-order term in Eq. (6).
3. The roots of B represent the *in vacuo* flexural wavenumbers in the cylindrical shell. This is the first-order term in Eq. (4).

Box 4
Simplifications of elements of **L** for the high-frequency range using order analysis.

For obtaining the wavenumbers at high frequencies, we substitute Ω by Ω/ϵ, where ϵ is a small number ($0<\epsilon\ll 1$). For the coupled wavenumber near the *in vacuo* flexural wave we substitute κ by $\kappa/\sqrt{\epsilon}$, whereas for the coupled wavenumber near the acoustic waves we substitute κ by κ/ϵ. Thus, we have the following two cases.

1. For the bending wave we have

$$L_{11}=-\Omega^2+\kappa^2+(1-\nu)/2\approx\mathcal{O}(1/\epsilon^2)+\mathcal{O}(1/\epsilon),L_{12}=L_{21}\approx\mathcal{O}(1/\sqrt{\epsilon}),$$

$$L_{33}\approx\mathcal{O}(1/\epsilon^2)+\mathcal{O}(1/\epsilon^2)+\mathcal{O}(\mathscr{F})\approx\mathcal{O}(1/\epsilon^2)\text{or more depending on the order of}\mathscr{F},$$

$$L_{22}\approx\mathcal{O}(1/\epsilon^2),L_{23}=L_{32}=\mathcal{O}(1),L_{13}=L_{31}=\mathcal{O}(1/\sqrt{\epsilon}).$$

We choose to keep terms of $\mathcal{O}(1/\epsilon)$ or higher. Thus, all off-diagonal terms are discarded. Also, within the diagonal terms we have the following simplifications:

$$L_{11}=-\Omega^2+\kappa^2,L_{22}=-\Omega^2+\frac{1-\nu}{2}\kappa^2,L_{33}=-\Omega^2+\beta^2\kappa^4+\mathscr{F}. \tag{12}$$

2. For the acoustic waves we have

$$L_{11}=-\Omega^2+\kappa^2+(1-\nu)/2\approx\mathcal{O}(1/\epsilon^2),L_{12}=L_{21}\approx\mathcal{O}(1/\epsilon),$$

$$L_{33}\approx\mathcal{O}(1/\epsilon^2)+\mathcal{O}(1/\epsilon^4)+\mathcal{O}(\mathscr{F})\approx\mathcal{O}(1/\epsilon^4)\text{or more depending on the order of }\mathscr{F},$$

$$L_{22}=\approx\mathcal{O}(1/\epsilon^2),L_{23}=L_{32}=\mathcal{O}(1),L_{13}=L_{31}=\mathcal{O}(1/\epsilon).$$

We choose to keep the term of $\mathcal{O}(1/\epsilon^2)$ or higher. Thus, all off-diagonal terms are discarded. Also, within the diagonal terms we have the same simplifications as given in Eq. (12).

Thus, for the high-frequency analysis, we shall choose the off-diagonal terms to be zero and the diagonal terms to be given by Eq. (12).

4. The roots of R are the wavenumbers corresponding to the cut-on modes of the rigid-walled acoustic duct (see Eq. (1a)).
5. The roots of P are the wavenumbers corresponding to the cut-on modes of the pressure-release acoustic duct (see Eq. (1b)).

It may be seen from Eq. (13) that the longitudinal and the torsional wavenumbers are not affected by fluid-loading at first order. A subset of Eq. (13) (repeated below) gives the coupled flexural and acoustic wavenumbers

$$\left[\overbrace{(-\Omega^2+\beta^2\kappa^4)}^{B}\xi\overbrace{J_1'(\xi)}^{R}-\mu\Omega^2\underbrace{J_1(\xi)}_{P}\right]=0. \tag{14}$$

Note, that with $\mu=0$, a root of Eq. (14) is given by $\xi=0$, which is the plane wave solution. At this condition, a trivial solution is obtained since $p(r,\theta)=J_1(\sqrt{\omega^2/c_f^2-k_x^2}r)\cos(\theta)=J_1(0)\cos(\theta)$ is zero throughout the cylindrical cavity.

3.1.1. Small μ

3.1.1.1. Coupled bending wavenumber $\kappa_B(\mu)$. The coupled bending wavenumber is given by

$$\kappa_B(\mu) = \sqrt{\frac{\Omega}{\beta}} + \underbrace{\frac{1}{4\beta^2} \frac{\Omega^2 J_1\left(\sqrt{\frac{\Omega(c^2\Omega\beta-1)}{\beta}}\right)\left(\frac{\beta}{\Omega}\right)^{3/2}}{\sqrt{\frac{\Omega(c^2\Omega\beta-1)}{\beta}} J_1'\left(\sqrt{\frac{\Omega(c^2\Omega\beta-1)}{\beta}}\right)}}_{\text{correction factor}} \mu + \mathcal{O}(\mu^2), \text{ where } c = \frac{c_L}{c_f}. \tag{15}$$

Details of the derivation are presented in Box 5. Thus, at first order, $\kappa_B(\mu)$ gives the *in vacuo* bending wavenumber (as in Eq. (4)). The μ-dependent correction factor captures the fluid-loading effect. It is mass-like when positive and stiffness-like when negative.

The *in vacuo* bending wavenumber intersects the wavenumber corresponding to rigid-walled cut-ons at Ω_n^r ($n = 1, 2, \ldots$), the rigid-duct coincidences. At these frequencies, from Eq. (1a) $J_1'(\sqrt{c^2\Omega^2 - \kappa^2}) = 0$. Moreover, the flexural wavenumber $\kappa \approx \sqrt{\Omega/\beta}$ at these coincidences. Using these values we have, $J_1'(\sqrt{c^2\Omega^2 - \Omega/\beta}) = 0$, and thus the denominator of Eq. (15) approaches zero and the expression becomes invalid.

Similar invalidations of asymptotic solutions around certain frequencies occur at various places in the subsequent derivations. This type of breakdown of a solution is typical in asymptotic methods. A detailed description of the reasons can be found in Ref. [28, p. 8]. Here, we just mention that an alternative asymptotic expansion incorporating a different scaling of the asymptotic parameter can be found for the frequencies (like Ω_n^r) where the basic asymptotic expansion fails. Such alternative expansions have been worked out for the simpler case of plate geometry [17] and also for a fluid-filled cylindrical shell vibrating in the axisymmetric mode [18]. To keep the article length within limits, instead of a full derivation, we shall use a continuity argument to determine the nature of the coupled wavenumbers at frequencies (for e.g. $\Omega \approx \Omega_n^r$) where the basic asymptotic solution fails.

Similarly, the numerator of the correction term approaches zero at the frequencies where the wavenumber of the *in vacuo* bending wave equals that of the pressure-release acoustic cut-ons. These pressure-release

Box 5

Derivation of the asymptotic expressions for the coupled wavenumbers $\kappa_B(\mu)$ and $\kappa_1^r(\mu)$ at high frequencies for small μ.

We use $J_1'(x) = J_0(x) - J_1(x)/x$ in Eq. (14) and substitute $\kappa = a_0 + a_1\mu$. Series expansion about μ gives an equation involving various orders of μ. The equation at $\mathcal{O}(1)$ has a solution $a_0 = \sqrt{\Omega/\beta}$ corresponding to the *in vacuo* flexural wave. Using this value for a_0, we get at $\mathcal{O}(\mu)$ the following solution for a_1:

$$a_1 = \frac{1}{4\beta^2} \frac{\Omega^2 J_1\left(\sqrt{\frac{\Omega(c^2\Omega\beta-1)}{\beta}}\right)\left(\frac{\beta}{\Omega}\right)^{3/2}}{\sqrt{\frac{\Omega(c^2\Omega\beta-1)}{\beta}} J_1'\left(\sqrt{\frac{\Omega(c^2\Omega\beta-1)}{\beta}}\right)}.$$

Similarly,the $\mathcal{O}(1)$ equation has roots a_0 such that $J_1'(\sqrt{c^2\Omega^2 - a_0^2}) = 0$. These are the wavenumbers for the rigid-walled acoustic duct (see Eq. (1a)). For each value of a_0 found, the value of the corresponding a_1 may be obtained from the $\mathcal{O}(\mu)$ equation. For example, for the first cut-on wave $a_0 = \sqrt{c^2\Omega^2 - 1.841^2}$ and

$$a_1 = \frac{0.5819\Omega^2}{0.4102(-\Omega^2 + \beta^2(c^2\Omega^2 - 3.389)^2)\sqrt{c^2\Omega^2 - 3.389}}.$$

coincidence frequencies will be denoted by Ω_n^p ($n = 1, 2, \ldots$), where n denotes the order of the cut-on. Note, $\Omega_1^r < \Omega_1^p < \Omega_2^r < \Omega_2^p \ldots$. The correction term switches sign at each pressure-release coincidence (Ω_n^p). Hence, the nature of fluid-loading (in the form of additional mass or stiffness on the structure) changes on either side of Ω_n^p. At Ω_n^p, the correction term being zero, the effect of fluid-loading is not perceived by the structure.

The correction factor to the *in vacuo* bending wavenumber caused due to the fluid-loading effect is plotted in Fig. 7. Thus, below Ω_1^r (in the figure we have shown till $\Omega = 7$) the fluid-loading is mass-like, while above Ω_1^r the fluid-loading nature is alternately mass-like and stiffness-like. The presence of alternate mass-loading and stiffness-loading frequency regions is typical in structural systems. As examples, we may cite the following examples: spring-mass system backed by an acoustic cavity [22], two-dimensional waveguide [17], fluid-filled cylindrical shell vibrating in the axisymmetric mode [18].

In Fig. 8a, we compare the asymptotic solution obtained in Eq. (15) with that obtained through numerical solution of the coupled dispersion equation (11) for $\mu = 0.2$. Due to the reasons cited above, the plot is done in two parts (a) frequency below $\Omega_1^r \approx 7.7$ (b) frequency between 7.8 ($> \Omega_1^r$) and $8.05 < \Omega_2^r$. The frequency range $7.7 < \Omega < 7.8$ is left out in the above plot as this frequency range is near Ω_1^r and hence the asymptotic solution is not applicable in this range. A schematic presentation of these results is shown in Fig. 9a.

3.1.1.2. Coupled acoustic rigid-duct wavenumber ($\kappa_1^r(\mu)$). $\kappa_1^r(\mu)$ (see Table 2 for notation) is given by

$$\kappa_1^r(\mu) = \sqrt{\frac{c_L^2\Omega^2}{c_f^2} - 3.389} + \underbrace{\left[\frac{0.5819\Omega^2}{0.4102(-\Omega^2 + \beta^2(c^2\Omega^2 - 3.389)^2)\sqrt{c^2\Omega^2 - 3.389}}\right]}_{\text{correction factor}} \mu + \mathcal{O}(\mu^2). \tag{16}$$

Detailed derivation is shown in Box 5.

For the frequency range below Ω_1^r, the *in vacuo* bending wavenumber is greater than the uncoupled rigid-duct acoustic wavenumber and *vice-versa*. Approximating the *in vacuo* bending wavenumber as $\sqrt{\Omega/\beta}$ (first-order estimate from Eq. (4)), we find that below Ω_1^r we have $\Omega^2 > \beta^2(c^2\Omega^2 - 3.389)^2$ which makes the correction factor negative. Thus, the structure increases the speed (and hence incompressibility) of the fluid in this frequency range. As the coupled wavenumber is decreased, this implies that the cut-on frequency is increased due to the presence of the flexible structure. Similarly, for frequencies above Ω_1^r we have $\Omega^2 < \beta^2(c^2\Omega^2 - 3.389)^2$ which makes the correction factor positive. Hence, the sonic speed of the fluid decreases implying that the influence of the structure is in the form of additional mass on the fluid.

At frequencies near Ω_1^r and the uncoupled cut-on frequency, the denominator approaches zero and hence the correction factor blows up making the asymptotic expansion invalid near this frequency. An alternative

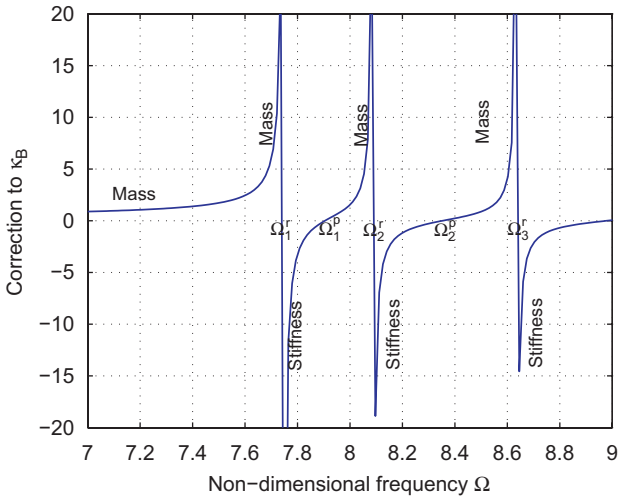

Fig. 7. Correction of the coupled structural wavenumber ($\kappa_B(\mu)$) over the *in vacuo* bending wavenumber (κ_B) at high frequencies due to small fluid-loading (μ). Parameters chosen are $h/a = 0.05$, $c_L/c_f = 3$.

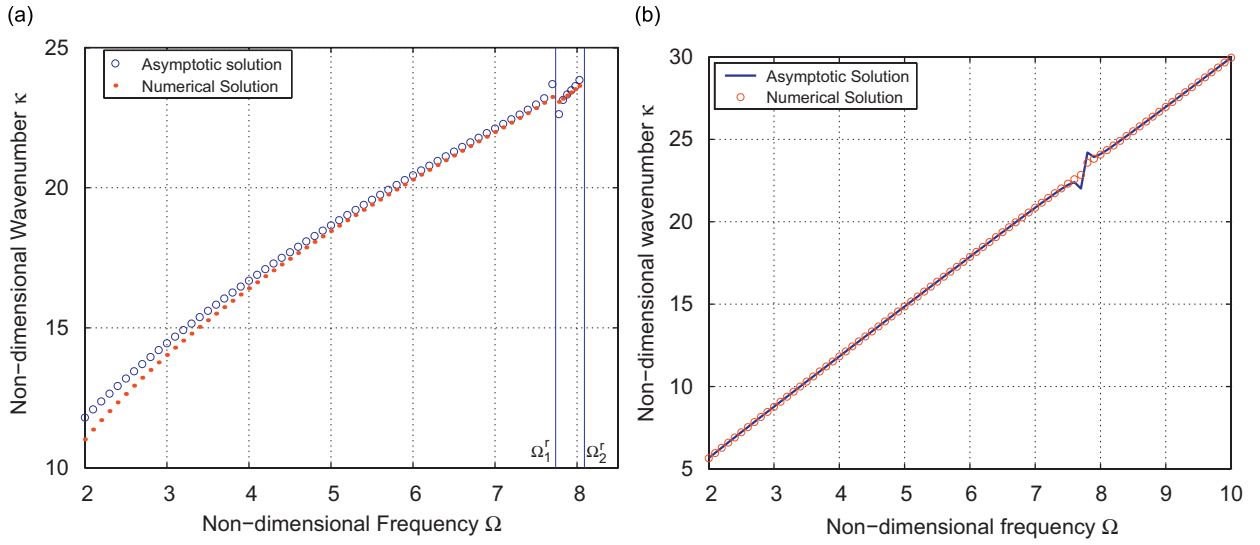

Fig. 8. Coupled wavenumbers for high frequencies and small μ. The parameters chosen are $h/a = 0.05$, $\nu = 0.25$, $\mu = 0.2$, $c_L/c_f = 3$. (a) $\kappa_B(\mu)$ for $\Omega < \Omega_1^r$ and $\Omega_1^r < \Omega < \Omega_2^r$. In the range $\Omega \approx \Omega_1^r$ and $\Omega \approx \Omega_2^r$, the asymptotic expression for $\kappa_B(\mu)$ found are invalid. (b) $\kappa_1^r(\mu)$. The figure indicates that the asymptotic expression turns invalid near Ω_1^r (the kink region near $\Omega \approx 7.75$).

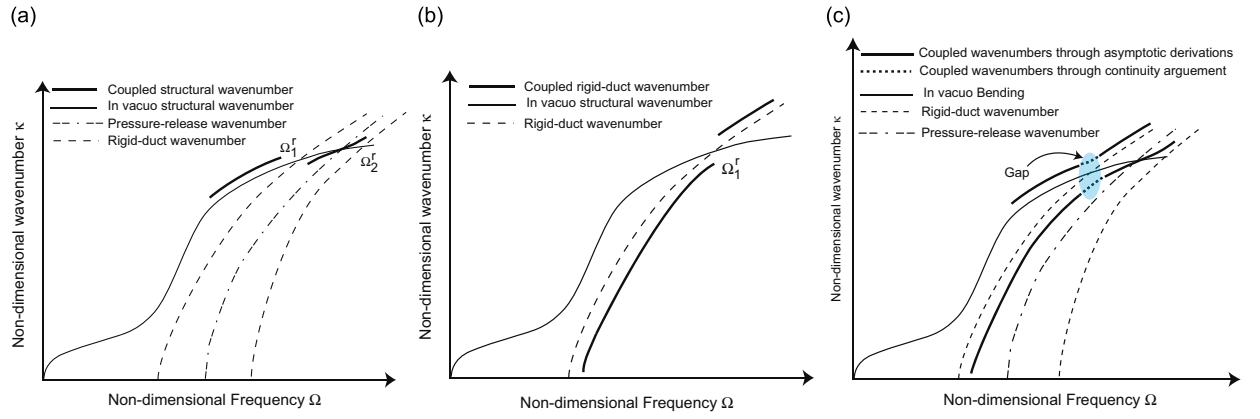

Fig. 9. Qualitative nature of the coupled wavenumbers at high frequencies with small μ. Also shown in the figure is the frequency range of validity of the asymptotic expressions obtained. (a) $\kappa_B(\mu)$ obtained from Eq. (15). (b) $\kappa_1^r(\mu)$ obtained from Eq. (16). (c) Coupled wavenumbers obtained through the asymptotic derivations and the continuity argument for the intermediate frequency range where the asymptotics does not hold good.

scaling of the asymptotic parameter can give us a valid asymptotic solution for $\Omega \approx \Omega_1^r$ [17,18]. Without actually deriving it, we shall employ an intuitive continuity argument for determining the coupled wavenumbers in the range $\Omega \approx \Omega_1^r$.

The function given by the equation above is plotted in Fig. 8b along with the numerical solution of the exact coupled dispersion equation (11) for $\mu = 0.2$. From the plot it is clear that the asymptotic solution turns invalid at frequencies near $\Omega_1^r \approx 7.75$. A schematic of the results found for the coupled rigid-duct wavenumber at high frequencies and small μ limit is presented in Fig. 9b.

3.1.1.3. Continuity argument. It was earlier stated that at frequencies where the regular asymptotic expansion fails (viz. Ω_n^r) there are alternative expansions possible. Such expansions have been presented in detail in Refs. [17,18]. Here we just mention that the coupled structural wavenumber branch below Ω_n^r joins with the coupled rigid-duct (nth mode) wavenumber branch above Ω_n^r. Likewise, the coupled rigid-duct (nth mode) wavenumber branch below Ω_n^r joins with the coupled structural wavenumber branch above Ω_n^r.

This creates a *gap* around the coincidence frequency region with each physical branch (coupled structural or coupled acoustic) encountering a *jump* at these frequencies. This is indicated in Fig. 9c (and repeated again in Fig. 11a). This type of effect was also observed by Cabelli [15] and in our earlier works [17,18].

3.1.2. Large μ

3.1.2.1. Coupled pressure-release wavenumber ($\kappa_1^p(\mu)$). To model the effect of the large fluid-loading parameter, we make the transformation $\mu' = 1/\mu$ in Eq. (14), where $0<\mu' \ll 1$. This results in the following equation:

$$\mu'(-\Omega^2+\beta^2\kappa^4)\sqrt{c^2\Omega^2-\kappa^2}J_1'(\sqrt{c^2\Omega^2-\kappa^2})-\Omega^2 J_1(\sqrt{c^2\Omega^2-\kappa^2})=0, \text{ where } c=\frac{c_L}{c_f}. \tag{17}$$

Clearly, for $\mu'=0$ the solutions are the acoustic wavenumbers of the pressure-release duct. With $0<\mu'\ll 1$, we expect coupled wavenumbers solutions to be close to these. We shall demonstrate the method for the first pressure-release cut-on denoted by $\kappa_1^p(\mu)$.

The details of the derivation are presented in Box 6. The final expression is

$$\kappa_1^p(\mu)=\sqrt{c^2\Omega^2-3.832^2}+\underbrace{\left[\frac{3.832^2(\Omega^2-\beta^2(c^2\Omega^2-3.832^2)^2)}{\Omega^2\sqrt{c^2\Omega^2-3.832^2}}\right]}_{\text{correction factor}}\frac{1}{\mu}. \tag{18}$$

This expression is valid for all frequencies except the first cut-on frequency of the pressure-release duct, where the denominator of the correction factor turns zero. Also, note that at the frequency of coincidence

Box 6
Derivation of the asymptotic expression for the coupled pressure-release wavenumber $\kappa_1^p(\mu)$ for the high-frequency range with large μ.

Substituting $\kappa = a_0 + a_1\mu'$ in Eq. (17) and performing a series expansion about μ' we get

$$\begin{aligned}&-\Omega^2 J_1(\sqrt{c^2\Omega^2-a_0^2})\\&+\left[(-\Omega^2+\beta^2a_0^4)\sqrt{c^2\Omega^2-a_0^2}J_1'(\sqrt{c^2\Omega^2-a_0^2})+\frac{1}{2}\frac{\Omega^2a_0a_1(J_0(\sqrt{c^2\Omega^2-a_0^2})-J_2(\sqrt{c^2\Omega^2-a_0^2}))}{\sqrt{c^2\Omega^2-a_0^2}}\right]\mu'\\&+\mathcal{O}(\mu'^2)\\&=0.\end{aligned}$$

Using $J_0(x)-J_2(x)=J_1'(x)$, we get

$$-\Omega^2 J_1(\sqrt{c^2\Omega^2-a_0^2})=0\Rightarrow a_0=\sqrt{c^2\Omega^2-3.832^2},$$

$$(-\Omega^2+\beta^2a_0^4)\sqrt{c^2\Omega^2-a_0^2}+\frac{\Omega^2a_0a_1}{\sqrt{c^2\Omega^2-a_0^2}}=0\Rightarrow a_1=\frac{3.832^2(\Omega^2-\beta^2a_0^4)}{\Omega^2a_0}. \tag{19}$$

Thus,

$$\kappa=\sqrt{c^2\Omega^2-3.832^2}+\left[\frac{3.832^2(\Omega^2-\beta^2(c^2\Omega^2-3.832^2)^2)}{\Omega^2\sqrt{c^2\Omega^2-3.832^2}}\right]\mu'.$$

between the *in vacuo* structural wave and the first acoustic pressure-release cut-on (denoted by Ω_1^p), we have $\Omega/\beta = c^2\Omega^2 - 3.832^2$. Thus, at the coincidence frequency, the correction factor is zero. For $\Omega < \Omega_1^p$, the structural wavenumber is greater than the acoustic wavenumber, hence the correction factor is positive, whereas for $\Omega > \Omega_1^p$, the correction factor is negative. This lowers the cut-on frequency. As before, the sign of the correction factor decides the mass/stiffness effect of the structure on the fluid wavenumber.

The expression in Eq. (18) is plotted in Fig. 10 along with the numerical solution of the exact coupled dispersion equation (11). In addition to $\kappa_1^p(\mu)$, a coupled wavenumber branch greater than the *in vacuo* structural wavenumber and the uncoupled wavenumber of the first rigid-duct cut-on mode exists when μ is large. Though by numerical solution this branch may be found, we have not been able to find the asymptotic expression corresponding to this branch. The existence of this branch has been established by Fahy [22] for the case of plane geometry. As we have observed, for high frequencies the dynamics of the cylinder is *locally* plate-like. Thus, Fahy's arguments can be extended for the present geometry also. From the small ε analysis, we observed that there is a wavenumber branch greater than κ_B and κ_1^r. The same branch exists as ε continuously increases to large values. Summarizing these observations, a schematic presentation of the results found for the coupled wavenumbers for high frequency and large μ is shown in Fig. 11b.

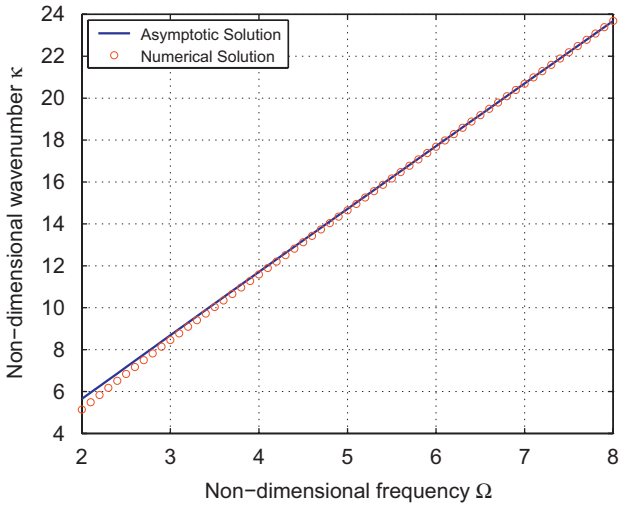

Fig. 10. Coupled wavenumber corresponding to the first pressure-release acoustic duct cut-on mode ($\kappa_1^p(\mu)$) valid for high frequencies and large μ. Parameters chosen are $h/a = 0.05$, $c_L/c_f = 3$, $\mu = 3$, $\nu = 0.25$.

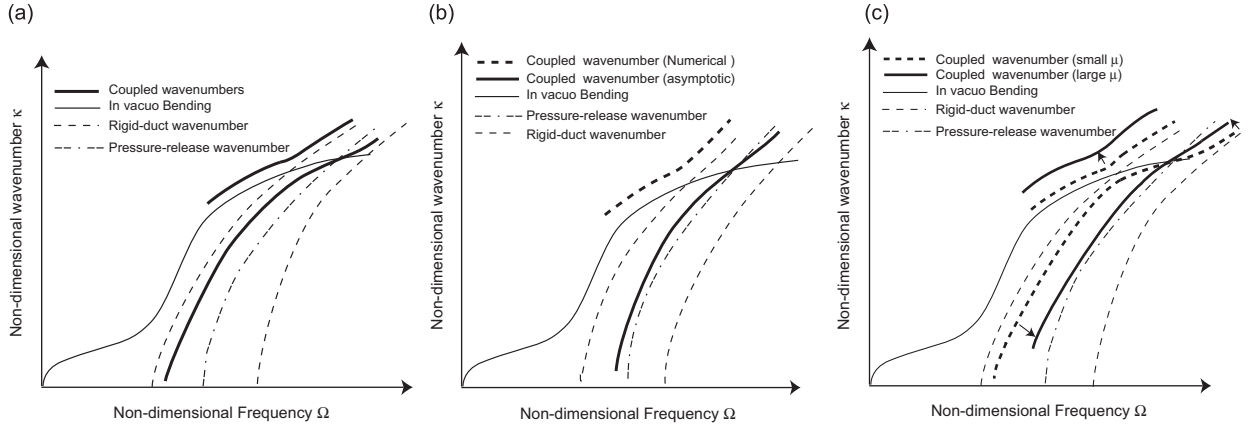

Fig. 11. Coupled wavenumbers of a fluid-filled cylindrical shell at high frequencies: (a) with small μ, (b) with large μ, (c) transition (indicated by arrows) from small μ to large μ.

3.1.3. Transition from small μ to large μ

From Figs. 11a and b, we may deduce the nature of transition of the coupled wavenumbers as μ increases from small to large values. This is indicated in Fig. 11c. A general trend observed is that for small μ, the coupled wavenumbers are close to the *in vacuo* structural and the rigid-duct acoustic wavenumbers. As μ increases, they get perturbed further away, until at large μ they can be better identified as perturbations to the wavenumbers of the pressure-release acoustic duct.

3.2. Low-frequency range

From our study of the *in vacuo* cylindrical shell in Section 2, it was noted that at low frequencies, the shell dynamics may be represented by the Timoshenko beam model. Physically, we know that the dynamics of the beam is largely unaffected by the Poisson's ratio (ν). This is also seen from Fig. 12 and hence, we shall choose $\nu = 0$ in this part of the derivations.

The simplified coupled dispersion equation in this case is (see Box 7 for details)

$$\underbrace{(-2\Omega^2+\kappa^4+\beta^2+4\beta^2\kappa^2-5\kappa^2\Omega^2)}_{\text{Timoshenko beam}}\,\xi\,\overbrace{J_1'(\xi)}^{R}-\mu\Omega^2\underbrace{J_1(\xi)}_{P}\overbrace{(2\kappa^2-3\Omega^2+\kappa^4-3\kappa^2\Omega^2+1)}^{\text{Complex wavenumbers}}=0. \tag{20}$$

3.2.1. Small μ ($\underline{\kappa_B}(\mu)$, $\kappa_1^r(\mu)$)

For $\mu = 0$, we get the *in vacuo* structural wavenumber ($\kappa_B \approx 2^{1/4}\sqrt{\Omega}$, for small β) and the wavenumber of the rigid-acoustic duct (given by the term R in the equation above). With $0<\mu\ll 1$, perturbations to these wavenumbers (denoted by $\underline{\kappa_B}(\mu)$ and $\kappa_n^r(\mu)$, respectively) will be derived. As with the high-frequency analysis, the roots of ξ represent the acoustic plane wave with zero pressure.

The final form of $\underline{\kappa_B}(\mu)$ is

$$\underline{\kappa_B}(\mu) = k_0 - \frac{\Omega^2 J_1(\sqrt{c^2\Omega^2-k_0^2})(1+2k_0^2-3\Omega^2+k_0^4-3k_0^2\Omega^2)}{(-10k_0\Omega^2+4k_0^3+8\beta^2k_0)\sqrt{c^2\Omega^2-k_0^2}J_1'(\sqrt{c^2\Omega^2-k_0^2})}, \tag{21}$$

where k_0 is the root of $x^4-5x^2\Omega^2+\beta^2-2\Omega^2+4\beta^2x^2=0$.

The process of derivation is similar to the earlier ones and hence not presented. Due to the J_1' term in the denominator of the correction factor, the asymptotic expression derived above again turns invalid at Ω_n^r.

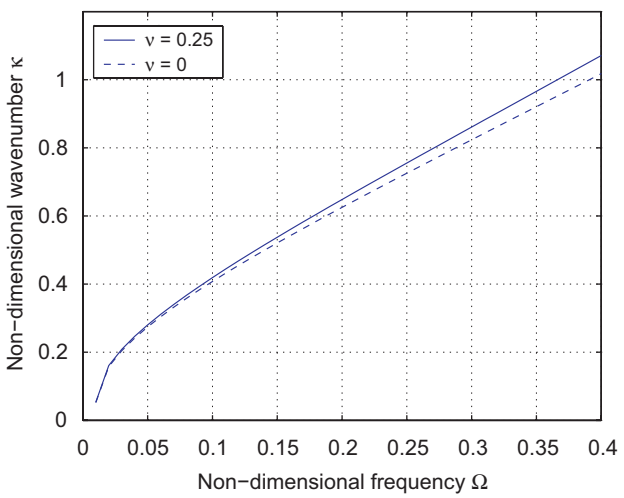

Fig. 12. Effect of Poisson's ratio on the low frequency *in vacuo* bending wavenumber.

Box 7
Simplification of the coupled dispersion Eq. (11) for the low-frequency range.

Note, the scaling for the fluid-loading term *viz.* $\mathscr{F} = -\mu\Omega^2 J_1(\xi)/\xi J_1'(\xi)$ is not known *a-priori*. We shall scale the remaining variables as $k = \kappa\sqrt{\epsilon}$ (since we are looking for solutions near flexural wavenumber), $\Omega' = \Omega\epsilon$ and $b = \beta\epsilon$. The determinant of the matrix **L** correct upto $\mathcal{O}(\epsilon^3)$ is

$$\tfrac{1}{2}\mathscr{F} + \epsilon k^2\mathscr{F} + \tfrac{1}{2}\epsilon^2 b^2 + \tfrac{1}{2}\epsilon^2 k^4\mathscr{F} - \Omega'^2\epsilon^2 - \frac{3}{2}\Omega'^2\epsilon^2\mathscr{F} + \tfrac{1}{2}\epsilon^2 k^4 + 2\epsilon^3 b^2 k^2 - \tfrac{5}{2}\epsilon^3 k^2\Omega'^2 - \tfrac{3}{2}\Omega'^2\epsilon^3 k^2\mathscr{F} = 0.$$

Thus,the approximate coupled dispersion equation valid for low frequencies is given by

$$-\Omega^2 + \tfrac{1}{2}\kappa^4 + \tfrac{1}{2}\beta^2 + 2\beta^2\kappa^2 - \tfrac{5}{2}\kappa^2\Omega^2 + (\kappa^2 - \tfrac{3}{2}\Omega^2 + \tfrac{1}{2}\kappa^4 - \tfrac{3}{2}\kappa^2\Omega^2 + \tfrac{1}{2})\mathscr{F} = 0.$$

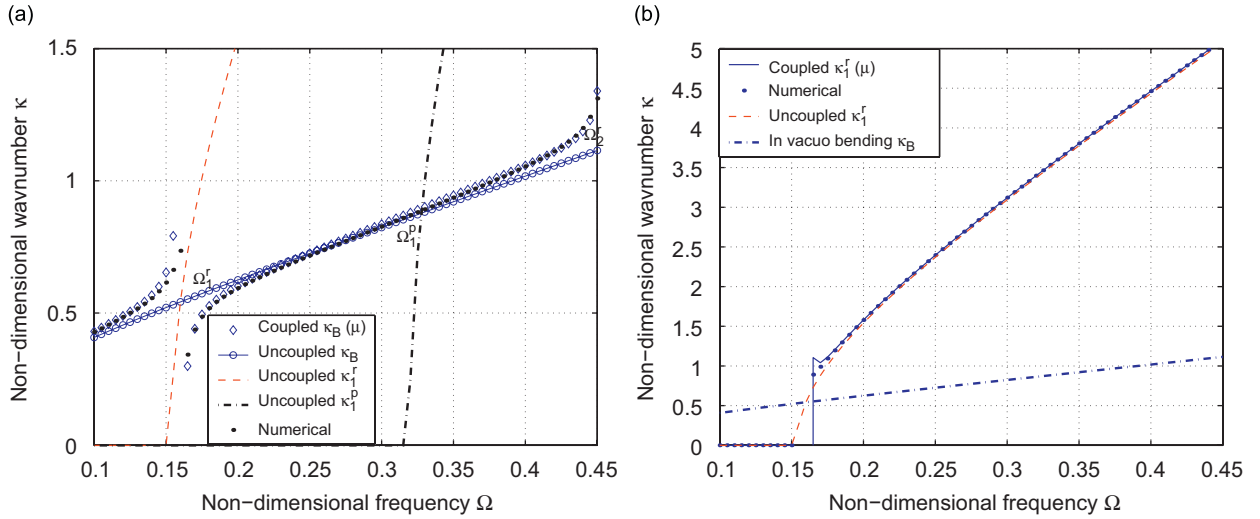

Fig. 13. Coupled wavenumbers for low frequencies and small μ. Parameters chosen are $c_L/c_f = 12$, $h/a = 0.05$. (a) $\underline{\kappa_B(\mu)}$ for $\mu = 0.25$ and (b) $\kappa_1^r(\mu)$ for $\mu = 0.5$.

The function obtained in Eq. (21) is plotted in Fig. 13a along with the numerical solution of the coupled dispersion equation (11). As explained earlier, the solution blows up at the frequencies Ω_1^r and Ω_2^r (at the end of the x-axis). The common features such as mass/stiffness loading of the structure by the fluid through sign change around Ω_1^p may be noted.

Similarly, the coupled rigid-duct acoustic wavenumber ($\kappa_1^r(\mu)$) can be obtained. The expression is too unwieldy to be presented here. The function is plotted in Fig. 13b along with the numerical solution of Eq. (11). As in the high-frequency analysis, the asymptotic expression obtained is invalid at frequencies close to the uncoupled cut-on frequency and the coincidence frequency Ω_1^r. It can be seen that the uncoupled cut-on frequency is nearly equal to the coincidence frequency for this case. Hence, the asymptotic expansion is valid only for $\Omega > \Omega_1^r$. Also, note that for $\Omega > \Omega_1^r$, the coupled wavenumber $\kappa_1^r(\mu)$ is greater than the corresponding uncoupled wavenumber κ_1^r. Through numerical analysis (not presented here) it is found that below Ω_1^r the coupled wavenumber $\kappa_1^r(\mu)$ is less than the corresponding uncoupled wavenumber κ_1^r and consequently the cut-on frequency is increased due to the fluid–structure coupling. These observations are thus similar to those obtained for the high-frequency analysis. A similar analysis can be carried for other cut-ons.

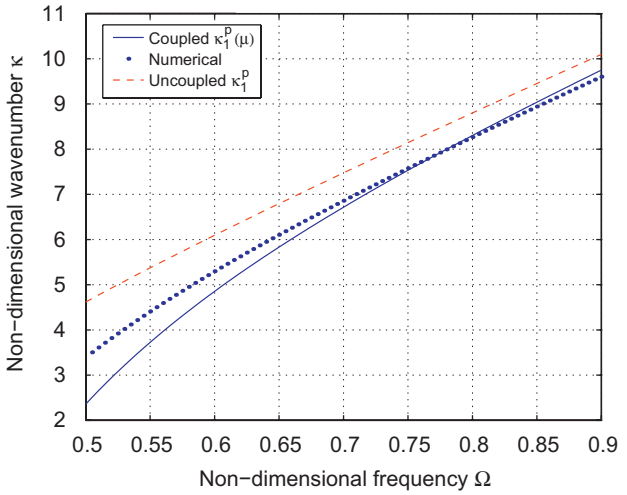

Fig. 14. Low-frequency coupled wavenumber for the first cut-on mode of the pressure-release acoustic duct ($\kappa_1^p(\mu)$). Parameters chosen are $c_L/c_f = 12$, $h/a = 0.05$, $\mu = 5$.

Using continuity arguments similar to that presented earlier, we can find the coupled wavenumber solutions (for both the structural and the acoustic wavenumbers) for $\Omega \approx \Omega_n^r$. A schematic of the complete results obtained for the case of low frequency small fluid-loading parameter is shown in Fig. 15a.

3.2.2. *Large μ ($\kappa_1^p(\mu)$)*

As $\mu \to \infty$ in Eq. (20), the solution approaches the wavenumber of the pressure-release acoustic duct. For large μ, the coupled wavenumbers ($\kappa_1^p(\mu)$) may be found as perturbations to these. The procedure is similar to that presented in the high-frequency analysis. The expression obtained in this case is too unwieldy to be presented here. A plot of the expression is shown in Fig. 14 along with the numerical solution. As with the high-frequency analysis, the asymptotic expression for this case is valid beyond the cut-on frequency (for Fig. 14 this is $\Omega > 0.5$). In this range, the coupled wavenumber ($\kappa_1^p(\mu)$) is less than the uncoupled pressure-release wavenumber (κ_1^p). Also, through numerical analysis it is verified that analogous to the high-frequency analysis, below Ω_1^p, $\kappa_1^p(\mu) > \kappa_1^p$ and consequently the cut-on frequency is decreased due to the coupling.

Also, note that the polynomial term multiplying the J_1 term in Eq. (20) does not have any real root. Thus, the only real root for the coupled system is that described above.

Similar to the high-frequency analysis, we have numerically obtained a coupled wavenumber branch greater than the *in vacuo* structural wavenumber and the wavenumber of the first rigid-duct cut-on. We have been unable to obtain the asymptotic expression corresponding to this branch. Summarizing these results we present a schematic for the low-frequency large μ derivations in Fig. 15b. As with the high-frequency analysis, the results of transition of low-frequency coupled wavenumbers from small to large μ is summarized in Fig. 15c.

4. Conclusions

In this article, coupled wavenumber solutions for a fluid-filled infinite cylindrical shell vibrating in the beam mode are found using an asymptotic method. While numerical solutions to this problem are known, use of the asymptotic method to find the analytical expressions is novel. The asymptotic method leads to coupled wavenumber expressions which are modifications over the *in vacuo* structural wavenumbers and the wavenumbers of the rigid-walled or pressure-release acoustic duct. The additional mass or stiffness effect perceived by the structure and the fluid due to the coupling effect is borne out by the sign of the correction factor. This approach provides better physical insights into the behavior of fluid–structure coupling in a curved geometry. Though this study was exclusively for the beam mode ($n = 1$), the method can be carried over to higher order modes ($n > 1$) also.

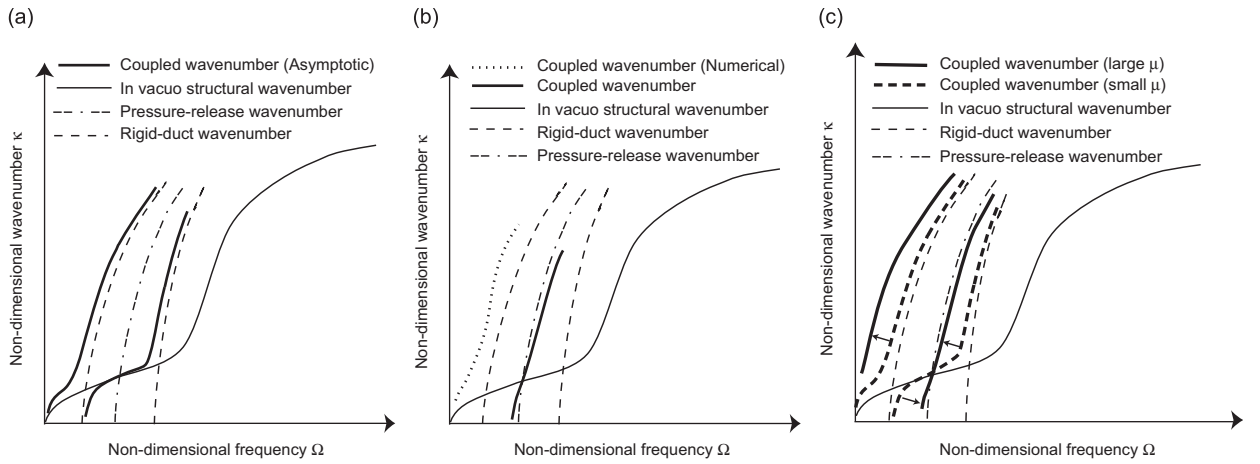

Fig. 15. Coupled wavenumber results obtained for low frequency: (a) small μ, (b) large μ, (c) transition (indicated by arrows) from small to large μ.

Initially, the uncoupled dispersion characteristics of the acoustic fluid and the cylindrical shell structure are presented. For the acoustic medium, closed form expression for the wavenumbers are well-known. However, for the *in vacuo* cylindrical shell, the dispersion relation is complicated and unwieldy. Using asymptotic methods, simple closed form expressions for the *in vacuo* shell wavenumbers (longitudinal, torsional and bending) are derived for low and high frequencies. It is shown that for low frequencies ($\Omega \ll 1$) the *in vacuo* shell behaves as a Timoshenko beam, whereas, for high frequencies ($\Omega \gg 1$) the shell behavior is like a plate of the same shell thickness.

For both the extremes of the frequency range, we find that under the influence of small fluid-loading (characterized by small μ) the corresponding *in vacuo* structural wavenumbers (longitudinal, bending and torsional) get modified. However, the coupling-effect is most dominant for the bending waves. The modification in the form of asymptotic expressions to the *in vacuo* bending wavenumber and the waveumbers of the uncoupled rigid acoustic duct are found for both high and low frequencies.

These asymptotic expressions are valid for all frequencies other than the rigid-duct coincidences (Ω_n^r) and the cut-on frequencies of the rigid acoustic duct. Near the coincidence frequencies we use a continuity argument to prove that the structural wavenumber branch below coincidence merges with the acoustic branch beyond coincidence and *vice-versa*. This creates a gap in the coincidence frequency region. Such a phenomenon is commonly known as the curve-veering effect in literature. Also, it is found that the cut-on frequency of the rigid acoustic duct increases due to the presence of the structure.

The other extreme of large fluid-loading (characterized by large μ) is also analyzed separately for high and low frequencies and appropriate analytical expressions are derived. It is found that the coupled wavenumbers in this case are perturbations of the wavenumbers of the pressure-release acoustic duct. Also, beyond the pressure-release coincidences (Ω_n^p) the coupled wavenumbers are less than the uncoupled pressure-release wavenumbers and *vice-versa*. The cut-on frequency of the pressure-release acoustic duct decreases due to the fluid–structure coupling.

For all frequencies and for all μ, there exists a coupled wavenumber branch greater than any of the uncoupled wavenumbers. Fahy [22] showed the existence of this coupled wavenumber branch for the case of a flat plate. We have found asymptotic expressions (for both high- and low-frequency limits) for this branch for the small μ case. For large μ, this branch was found numerically.

From the final results obtained (see Fig. 16), we observe that the nature of the coupled wavenumbers is qualitatively identical for both high and low frequencies. The difference lies in the behavior of the cylindrical shell structure. For low frequencies, the shell has a beam-like dynamics (the cross-section moves in unison in the transverse direction) whereas for high frequencies the structure has plate-like dynamics (each point in the cross-section moves in the radial direction) [19]. The general trend for small μ is that the coupled wavenumbers are close to the *in vacuo* structural wavenumber and the wavenumbers of the rigid-acoustic duct. With

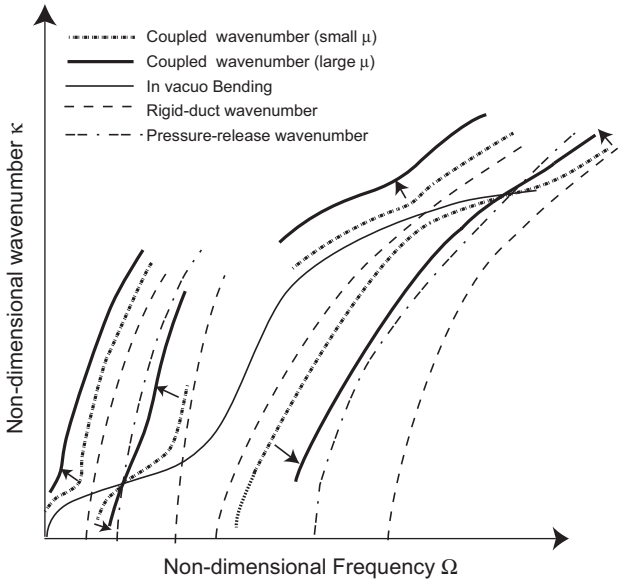

Fig. 16. The coupled wavenumber solutions found for high and low frequencies. Arrows indicate transition of solutions as the fluid-loading parameter increases.

increasing μ, the perturbation increases until the coupled wavenumbers are better identified as perturbations to the pressure-release wavenumbers.

Acknowledgment

We thank the reviewers for the time, effort and valuable comments. Due to their suggestions, the quality of the article has improved.

References

[1] C.R. Fuller, F.J. Fahy, Characteristics of wave propagation and energy distributions in cylindrical elastic shells filled with fluid, *Journal of Sound and Vibration* 81 (4) (1982) 501–518.
[2] G. Pavic, Vibrational energy flow in elastic circular cylindrical shells, *Journal of Sound and Vibration* 142 (2) (1990) 293–310.
[3] L. Feng, Acoustic properties of fluid-filled elastic pipes, *Journal of Sound and Vibration* 176 (3) (1994) 399–413.
[4] M. Maess, N. Wagner, L. Gaul, Dispersion curves of fluid-filled elastic pipes by standard FE models and eigen path analysis, *Journal of Sound and Vibration* 296 (2006) 264–276.
[5] A.H. Nayfeh, *Problems in Perturbation*, Wiley, New York, 1985.
[6] D. Blackstock, M. Hamilton, *Nonlinear Acoustics*, Academic Press, New York, 1998.
[7] P.M. Morse, K.U. Ingard, *Theoretical Acoustics*, McGraw-Hill Book Company, New York, 1968.
[8] D.G. Crighton, The 1988 Rayleigh medal lecture: fluid loading—the interaction between sound and vibration, *Journal of Sound and Vibration* 133 (1) (1989) 1–27.
[9] C.J. Chapman, S.V. Sorokin, The forced vibration of an elastic plate under significant fluid loading, *Journal of Sound and Vibration* 281 (2005) 719–741.
[10] J.F.M. Scott, The free modes of propagation of an infinite fluid-loaded thin cylindrical shell, *Journal of Sound and Vibration* 125 (2) (1988) 241–280.
[11] Y.P. Guo, Asymptotic solutions for helical wavenumbers of waves in fluid-loaded cylindrical shells, *Wave Motion* 22 (1995) 97–107.
[12] L. Huang, Y.S. Choy, R.M.C. So, T.L. Chong, Experimental study of sound propagation in a flexible duct, *Journal of the Acoustical Society of America* 108 (2) (2000) 624–631.
[13] S. Choi, Y.H. Kim, Sound wave propagation in a membrane duct, *Journal of the Acoustical Society of America* 112 (5) (2002) 1749–1752.
[14] M.K. Au-Yang, The hydrodynamic mass at frequencies above coincidence, *Journal of Sound and Vibration* 86 (2) (1983) 288–292.
[15] A. Cabelli, The propagation of sound in a square duct with a non-rigid side wall, *Journal of Sound and Vibration* 103 (3) (1985) 379–394.

[16] S.H. Ko, Sound wave propagation in a two dimensional flexible duct in the presence of an inviscid flow, *Journal of Sound and Vibration* 175 (2) (1994) 279–287.
[17] A. Sarkar, V.R. Sonti, An asymptotic analysis for the coupled dispersion characteristics of a structural acoustic waveguide, *Journal of Sound and Vibration* 306 (2007) 657–674.
[18] A. Sarkar, V.R. Sonti, Asymptotic analysis for the coupled wavenumbers in an infinite fluid-filled flexible cylindrical shell: the axisymmetric mode, *Computer Modeling in Engineering and Sciences* 21 (3) (2007) 193–207.
[19] C.R. Fuller, The effect of wall discontinuities on the propagation of flexural waves in cylindrical shells, *Journal of Sound and Vibration* 75 (2) (1981) 207–228.
[20] A. Leissa, Vibration of shells, Technical Report NASA SP-288, 1973.
[21] L.H. Donell, *Beams, Plates and Shell*, McGraw-Hill Book Company, New York, 1976.
[22] F.J. Fahy, *Sound, Structure and their Interaction: Radiation, Transmission and Response*, Academic Press, London, 1989.
[23] S. Timoshenko, D.H. Young, *Vibration Problems in Engineering*, D. Van Nostrand Co, Princeton, 1955.
[24] A. Kornecki, A note on beam-type vibrations of circular cylindrical shells, *Journal of Sound and Vibration* 14 (1) (1971) 1–6.
[25] K. Graff, *Wave Motion in Elastic Solids*, Clarendron Press, Oxford, 1975.
[26] R.D. Blevins, *Formulas for Natural Frequencies and Mode Shapes*, Van Nostrand Reinhold Company, New York, 1979.
[27] K. Forsberg, Axisymmetric and beam-type vibrations of thin cylindrical shells, *AIAA Journal* 7 (2) (1969) 221–227.
[28] E.J. Hinch, *Perturbation Methods*, Cambridge University Press, Cambridge, 1991.